A R C H I V E S O F M E T A L L U R G Y A N D M A T E R I A L S
Volume 57 2012 Issue 4
DOI: 10.2478/v10172-012-0136-y

W. PIEKARSKA*, M. KUBIAK*, Z. SATERNUS*

NUMERICAL MODELLING OF THERMAL AND STRUCTURAL STRAIN IN LASER WELDING PROCESS

MODELOWANIE NUMERYCZNE ODKSZTAŁCEŃ CIEPLNYCH I STRUKTURALNYCH W PROCESIE SPAWANIA TECHNIKĄ LASEROWĄ

This work concerns numerical modelling of thermal and structural strain, resulting in heating and cooling of laser butt-welded joints. Numerical analysis of strain is carried out in Abaqus FEA. Through the use of additional author's subroutines, the structural strain caused by phase transformations during heating and cooling of welded elements is taken into account in the analysis. V.I. Machnienko models as well as Continuous Heating Transformation (CHT) and Continuous Cooling Transformation (CCT) diagrams for S355 steel are implemented into UEXPAN subroutine in order to determine the kinetics of phase transformation in the solid state. The model takes into account thermomechanical properties of the base material varying with temperature.

The paper presents results of numerical simulation of temperature field, predicted structural composition, thermal and structural strain in laser butt-welded joints.

Keywords: Laser welding, heat transfer, phase transformations, numerical modelling, isotropic strain

W pracy przedstawiono numeryczne modelowanie odkształceń cieplnych i strukturalnych, powstających podczas nagrzewania i chłodzenia, złącza spawanego doczołowo wiązką promieniowania laserowego. Analizę numeryczną odkształceń przeprowadzono w programie Abaqus FEA. Dzięki zastosowaniu dodatkowych autorskich aplikacji w analizie uwzględniono odkształcenia strukturalne wywoływane przemianami fazowymi podczas nagrzewania i chłodzenia spawanych elementów. Do wyznaczenia kinetyki przemian fazowych w stanie stałym zastosowano modele V.I. Machnienki oraz wykresy CTP^A i CTPc-S dla stali S355 implementowane do procedury UEXPAN. W modelu uwzględniono zmienne z temperaturą własności termomechaniczne spawanego materiału.

Przedstawiono wyniki symulacji numerycznych pola temperatury, prognozowanego numerycznie składu strukturalnego oraz odkształceń termicznych i strukturalnych w złączu spawanym doczołowo wiązką promienia laserowego.

1. Introduction

Welding technologies maintain at the forefront the most widely used manufacturing techniques of metal products and large-scale constructions [1]. With the support of both European and global economy promoting innovative solutions, advanced welding technologies are more often used in the industry, allowing the production speed up with maintained good quality of obtained welds in terms of durability and appearance, at reduced costs of production [2, 3]. Recently, laser beam welding is intensively developed, examined and implemented in wide range of applications due to a high welding speed with a small amount of molten material and a small zone of thermal influence achieved in the process [2]. Despite many advantages of laser welding, one of difficulties during welding of certain, even good weldable steels, is the formation of hardening structures caused by phase transformations and significant hardening of welded joint due to the high concentration of heat energy and high cooling rates [4]. During heating and cooling of laser welded joint, temperature field and phase transformations are the cause of isotropic deformation that generates welding stress [5, 6, 7]. Welding deformation exceeding permissible values may hinder or completely prevent the installation of construction parts and reduce their properties as well as esthetic of the weldment. Therefore, reduction of welding distortion, especially at long weldments, is one of the main problems faced by engineers that should be considered at the design stage by choosing appropriate welding parameters.

* INSTITUTE OF MECHANICS AND MACHINE DESIGN FOUNDATIONS, CZESTOCHOWA UNIVERSITY OF TECHNOLOGY, 42-200 CZESTOCHOWA, 73 DABROWSKIEGO STR., POLAND

Welding is a complex process which involves coupled thermomechanical phenomena occurring in a wide range of temperatures and has a direct impact on the quality of welded joint [5-12]. Over the past decades, there have been numerous numerical and experimental studies to predict welding distortion and residual stress [5-7]. Despite this, the problem of controlling and reducing welding distortion is currently one of the fundamental industrial problems. Therefore, numerical analysis of thermomechanical phenomena, including phase transformations in the solid state, under different heating and cooling conditions of the joint is crucial in prediction of welding distortion

The paper presents numerical modeling of thermal and structural strain occurring in laser butt-welded joints. Numerical simulations are performed in Abaqus FEA software based on finite element method [13, 14]. Thermomechanical properties changing with temperature are taken into account in numerical simulations.

Movable welding source power distribution is described using gaussian volumetric heat source model with the assumption of linear decrease in heat energy along laser beam penetration depth. Heat source model is implemented into ABAQUS/Standard solver using additional subroutine DFLUX written in FORTRAN. In order to analyze phase transformations in solid state HETVAL and UEXPAN subroutines are used, allowing the prediction of microstructure composition as well as thermal and structural strain in welded joints. Phase transformations in solid state considered during heating and cooling of S355 steel are analyzed using V.I. Machnienko mathematical models as well as CHT and CCT diagrams. Obtained results of numerical simulations of laser butt-welding process include: temperature field, structural composition as well as thermal and structural strain in welded joints.

2. Mathematical and numerical models

Modelling of temperature field, phase transformations in solid state as well as thermal and structural strain was performed for laser butt-welded thin plate made of S355 steel with chemical composition: 0.19 C, 1.05 Mn, 0.2 Si, 0.08 Cr, 0.11 Ni, 0.006 Al, 0.028 P, 0.02 S [%]. Scheme of considered system is presented in Fig. 1. Dimensions of the plate are L=200mm, s=100mm, g=2mm. Due to the symmetry of the analyzed area, half of the geometry is assumed in the model with thermal insulation in the plane of symmetry.

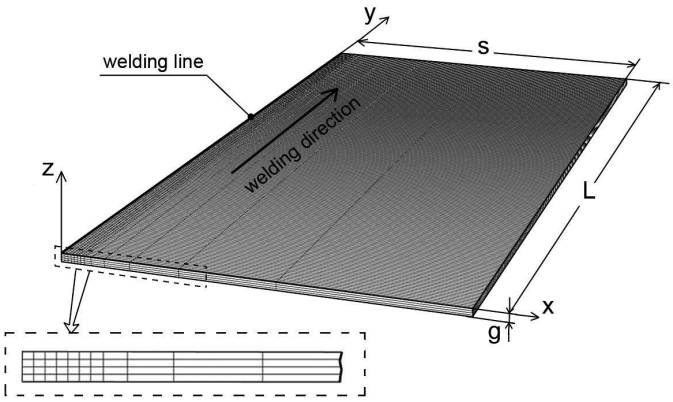

Fig. 1. Scheme of considered system witch finite element mesh used in calculations

2.1. Thermal analysis

Heat transfer in Abaqus/Standard is performed as „Uncoupled heat transfer" task, based on the energy conservation equation and Fourier's law [14] expressed in Lagrange's coordinates (without convective term). Temperature field $T = T(x_\alpha, t)$ in variational formulation is expressed as follows:

$$\int_V \rho \dot{U} \delta T \, dV + \int_V \frac{\partial \delta T}{\partial x_\alpha} \cdot \left(\lambda \frac{\partial T}{\partial x_\alpha} \right) dV = \int_V \delta T \, q_V dV + \int_S \delta T \, q_S dS \tag{1}$$

where $\lambda = \lambda(\mathrm{T})$ is a thermal conductivity [W/(m K)], U is a internal energy, q_v is laser beam heat source [W/m^3], q_S is a heat flux toward element surface [W/m^2], δT is a variational function, ρ is density [kg/m^3].

Equation (1) is completed by initial condition $t = 0 : T = T_o$ and boundary conditions. Boundary conditions of Dirichlet, Neumann and Newton type are accepted in numerical model of laser welding process with heat loss due to convection, radiation and evaporation as well as welding heat flux towards heated surface taken into account, according to the following formula:

$$q_S = -\lambda \frac{\partial T}{\partial n} = -q(r,0) + \alpha_k (T|_\Gamma - T_0) + \varepsilon \sigma (T|_\Gamma{}^4 - T_0^4) \tag{2}$$

where α_k is convective coefficient (assumed as α_k =150 W/(m^2°C), ε is radiation coefficient (ε =0.5), σ is Stefan-Boltzmann constant and $q(r,0)$ is the heat flux towards the top surface of welded workpiece (z =0) in the source activity zone of radius r, T_0 is an ambient temperature (assumed as 20 °C).

Internal energy U in equation (1) takes into account the latent heat of fusion (H_L) in the mushy zone (be-

tween T_S and T_L). Therefore, changes in specific heat $c(T) = dU / dT$ [J/(kg K)] are defined as:

$$c(T) = \begin{cases} c_S & \text{for} \quad T < T_S \\ \dfrac{c_S + c_L}{2} + \dfrac{H_L}{(T_L - T_S)} & \text{for} \quad T_S \leqslant T \leqslant T_L \\ c_L & \text{for} \quad T > T_L \end{cases} \tag{3}$$

Density in the mushy zone is calculated assuming linear approximation of solid fraction between solidus and liquidus temperatures (T_S =1477°C and T_L =1527°C), expressed as follows: $\rho_S = \rho_S f_S + \rho_L (1 - f_S)$, where ρ_S = 7800, ρ_L = 6800 kg/m^3, c_S = 650, c_L = 840 J/kg°C and H_L = 270×10^3 J/kg.

2.2. Heat source

Volumetric gaussian heat source model with assumed linear changes in energy distribution along material penetration depth [12] is used in calculations, defined as follows:

$$q_v(r,z) = \frac{Q}{\pi r_o^2 d} \exp\left[\left(1 - \frac{r^2}{r_o^2}\right)\right]\left(1 - \frac{z}{d}\right) \tag{4}$$

where Q is laser beam power [W], r_0 is beam radius [m], $r = \sqrt{x^2 + y^2}$ is actual radius [m], d is penetration depth [m], z is actual penetration [m].

Laser beam heat source model (4) is implemented into DFLUX subroutine where the motion of welding source is defined for every time increment as $x = v \cdot t$, where v is welding speed [m/min] and t is actual time [s]. Exemplary distribution of laser beam power is illustrated in Fig. 2 at the top surface and in cross section of welded joint.

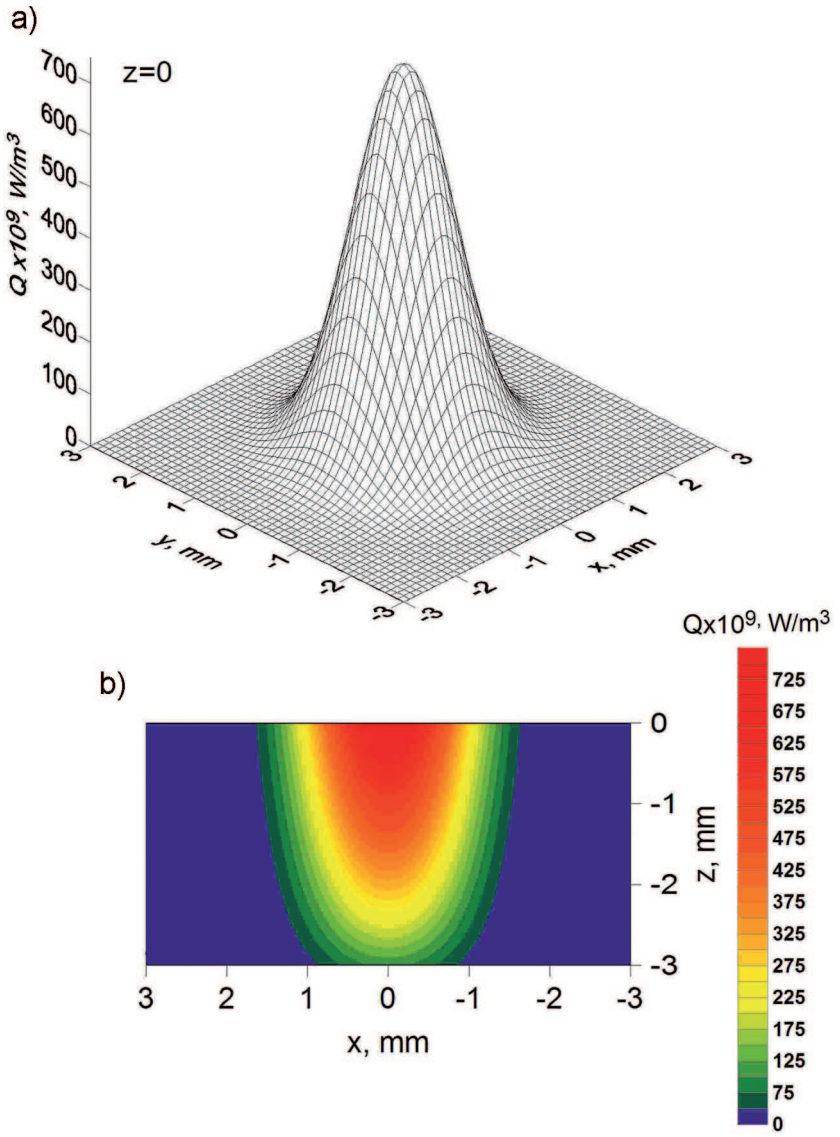

Fig. 2. Distribution of laser beam power a) at the top surface and b) in cross section of welded joint

2.3. Phase transformations in solid state. Thermal and structural strain

Numerical estimation of structure composition in laser welded joint is determined on the basis of classic mathematical models of kinetics of phase transformations [10, 15-21] in solid state as well as CHT diagram during heating and CCT diagram with final fractions of arising phases during cooling, obtained from dilatometric study of S355 steel [10].

Increase of volumetric fraction of austenite during heating in the range of austenitizing temperatures *Ac1(t)* and *Ac3(t)* is determined using V.I. Machnienko kinetics model [19]

$$\tilde{\eta}_A(T,t) = 1 - \exp(-k\frac{T_{sA} - T}{T_{sA} - T_{fA}}) \tag{5}$$

where T_{sA} and T_{fA} are start and final temperatures of austenite transformation, factor k is accepted in the range 2.5÷3.

Volumetric fractions of phases arising from austenite during cooling are determined by cooling time in temperatures range 800÷500 °C. Kinetics of diffusive phase transformations is also determined using V.I. Machnienko model [19]

$$\tilde{\eta}_i(T,t) = \eta^{\%}_{(\cdot)}\tilde{\eta}_A\left(1 - \exp\left(-k\frac{T^i_s - T}{T^i_s - T^i_f}\right)\right) \tag{6}$$

where $\eta^{\%}_{(\cdot)}$ is final fraction of structural constituent determined for specified cooling time in CCT diagram, $\underline{\eta}_A$ is a fraction of austenite formed during heating, T^i_s and T^i_f are start and final temperatures of i-th transformation, factor k is within the range 2.5÷3.

In the case of martensite transformation the volumetric fraction is determined using modified Koistinen-Marburger formula [20], expressed as follows:

$$\tilde{\eta}_M(T) = \eta^{\%}_{(\cdot)}\tilde{\eta}_A\left(1 - \exp\left(-k\left(\frac{M_s - T}{M_s - M_f}\right)^m\right)\right), \quad T \in [M_s, M_f(v_{8/5})] \tag{7}$$

where M_s and M_f are receptively start and final temperatures of martensite transformation, while k and m factors are determined experimentally.

Isotropic strain generated by temperature field and phase transformations in solid state during heating and cooling of laser welded joint is determined in increase form

$$d\varepsilon^{TPh} = \sum_i \alpha_i \eta_i dT - sign(dT)\sum_i \varepsilon^{Ph}_i d\eta_i \tag{8}$$

where i = A,F,P,B,M (austenite, bainite, ferrite, martensite and pearlite), $\alpha_i = \alpha_i(T)$ is thermal expansion coefficient for each phase, $\varepsilon^{Ph}_i = \varepsilon^{Ph}_i(T)$ is an isotropic structural strain resulting from the transformation of the base structure into austenite during heating and each phase (ferrite, pearlite, bainite or martensite) arising from austenite during cooling, $d\eta_i$ is a volumetric fractions of phases, sign (.) is a sign function. Thermal expansion coefficients and structural strain are determined on the basis of dilatometric analysis for S355 steel [10].

3. Computational model in Abaqus FEA

Basic version of Abaqus FEA engineering software does not allow the simulation of welding processes. Prediction of the structural composition of the weld as well as thermal and structural strain is possible only after the development of additional numerical procedures. Models of phase transformations in solid state and isotropic strain have been implemented into two numerical subroutines HETVAL and UEXPAN. HETVAL subroutine is used to determine maximum temperature of thermal cycle, which is then used to determine the fraction of austenite formed during heating (in the case of incomplete austenitization) as well as heating and cooling times (t_h and t_{8-5}). Thermal cycles parameters obtained in this subroutine are used as input data in UEXPAN procedure where kinetics of phase transformations in solid state and isotropic strain are calculated.

For determined heating and cooling rates austenitization temperatures (Ac_1, Ac_3) during heating, start (F_s, P_s, B_s, M_s) and final temperatures (F_f, P_f, B_f, M_f) of each phase transformation and final fractions of structure constituents during cooling are determined in UEXPAN subroutine. In this subroutine interpolated CHT and CCT diagrams are implemented with diagram of fractions of structural constituents (Fig. 3). Interpolation functions used in calculations are summarized in the Tables 1-2.

Structural composition of the joint and isotropic strain are estimated on the basis of adopted mathematical models and interpolated CHT and CCT diagrams. Presented in Table 3 thermal expansion coefficients ($\alpha_{(i)}$)of structural constituents and structural strain ($\varepsilon_{(i)}$) are determined experimentally, basing on dilatometric tests.

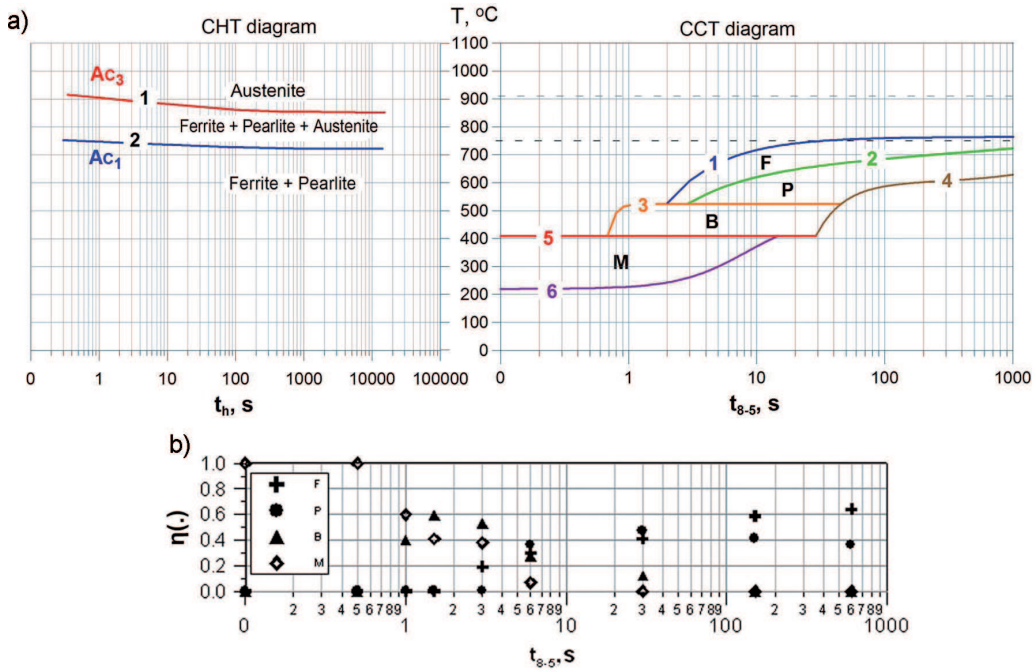

Fig. 3. Interpolated a) CHT and CCT diagrams and b) final fractions of structure constituents for S355 steel [10, 19]

TABLE 1

Interpolated CHT diagram

curve	time t_h	equation	coefficients
1 - A_{c1}	0.30 – 10000	$y = \frac{A \cdot B + C \cdot t_h^D}{B + t_h^D}$	A = 757.96 B = 2.66 C = 720.87 D = 0.57
2 - A_{c3}	0.30 – 10000	$y = \frac{A \cdot B + C \cdot t_h^D}{B + t_h^D}$	A = 926.36 B = 2.63 C = 850.90 D = 0.60

TABLE 2

Interpolated CCT diagram

curve	time t_h	equation	coefficients
1 - F_s	1.98 – 1000	$y = A_{Fs} + \frac{B_{Fs}}{t_{8-5}}$	A_{Fs} = 764.38 B_{Fs} = -473.38
2 - P_s	2.90 – 1000	$y = A_{Ps} \cdot B_{Ps}^{\frac{1}{t_{8-5}}} \cdot t_{8-5}^{C_{Ps}}$	A_{Ps} = 625.49 B_{Ps} = 0.56 C_{Ps} = 0.02
3 - B_s	0.69 – 46	$y = \frac{A_{Bs} \cdot B_{Bs} + C_{Bs} \cdot t_{8-5}^{D_{Bs}}}{B_{Bs} + t_{8-5}^{D_{Bs}}}$	A_{Bs} = -745.97 B_{Bs} = 0.0034 C_{Bs} = 523.30 D_{Bs} = 8.92
4 - P_f+B_f	29.10 – 1000	$y = A_{Pf+Bf} + B_{Pf+Bf} \cdot t_{8-5} + \frac{C_{Pf+Bf}}{t_{8-5}^2}$	A_{Pf+Bf} = 600.22 B_{Pf+Bf} = 0.03 C_{Pf+Bf} =-161246.52
5 - M_s	0.10 – 29.10	$y = A_{Ms} + B_{Ms} \cdot t_{8-5}$	A_{Ms} = 409 B_{Ms} = 0
6 - M_f	0.10 – 14.50	$y = \frac{A_{Ms} \cdot B_{Ms} + C_{Ms} \cdot t_{8-5}^{D_{Ms}}}{B_{Ms} + t_{8-5}^{D_{Ms}}}$	A_{Mf} =219.43 B_{Mf} = 32.36 C_{Mf} = 484.25 D_{Mf}= 1.64

TABLE 3

Thermal expansion coefficients and structural strains of S355 steel

Structural constituent	Thermal expansion coeff. $\alpha_{(i)}$, x10^{-6}, 1/°C		Structural strains $\varepsilon_{(i)}$, x10^{-3}	
austenite	α_A	21.0	ε_A	3.5
ferrite	α_F	14.7	ε_F	3.0
pearlite	α_P	13.7	ε_P	4.0
bainite	α_B	12.5	ε_B	3.5
martensite	α_M	12.0	ε_M	5.7

4. Results and discussion

Computer simulation of laser welding process was performed in Abaqus FEA for 200×100×2 mm thin plate (Fig. 1) made of S355 steel with assumed base material structure consist of ferritic – pearlitic structure (60% ferrite and 40% pearlite). Thermophysical parameters are summarized in Table 4. Assumed in calculations laser welding process parameters were set to: heat source power Q =1.3 kW, beam radius r_0 =0.9 mm, penetration depth d =1.7 mm and welding speed v =22 mm/s. In order to reduce computational time, symmetry of the joint was assumed in calculations. Dense finite element mesh was used in the heat sources activity zone because of the presents of large temperature gradients (Fig. 1).

Figures 4 and 5 show temperature profile in laser butt welded joint. Calculated temperature field in the cross section of the joint, presented in Fig. 5, allows the determination of weld and heat affected zone geometry. Material is completely melted if temperature reaches liquidus temperature (T_L). When temperature exceeds austenitization temperature T_g, the material is in the zone of structural transformations (heat affected zone). Below austenitization temperature welded material is treated as untransformed base material. Melted zone boundary is pointed out by solid line (liquidus isotherm T_L ≈1527°C), while dashed line determines heat affected zone boundary (average austenitization temperature Tg≈735°C).

TABLE 4

Termophysical properties assumed in calculations

Temperature [°C]	Conductivity λ [W/m °C]	Density ρ [kg/m^3]	Specific Heat c [J/kg°C]
20	52.0	7800	650
200	49.0	7800	650
1000	26.5	7800	650
1477	33.5	7800	650
1502	34.0	7300	745
1527	34.0	6800	840
2500	194.0	6800	840

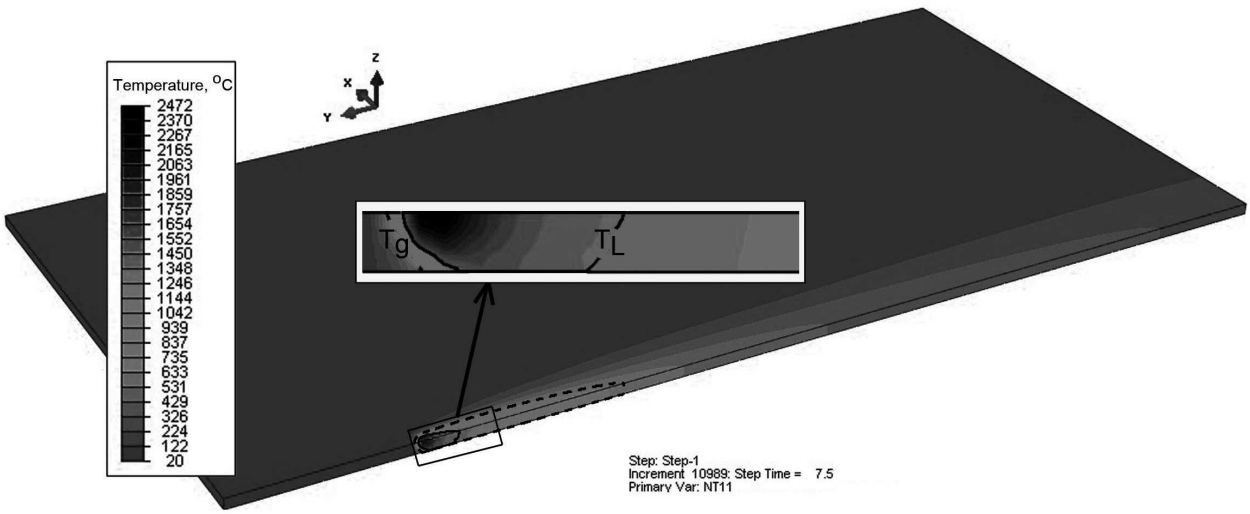

Fig. 4. Temperature profile in laser butt welded joint. Distribution at the top surface and in longitudinal section of the joint

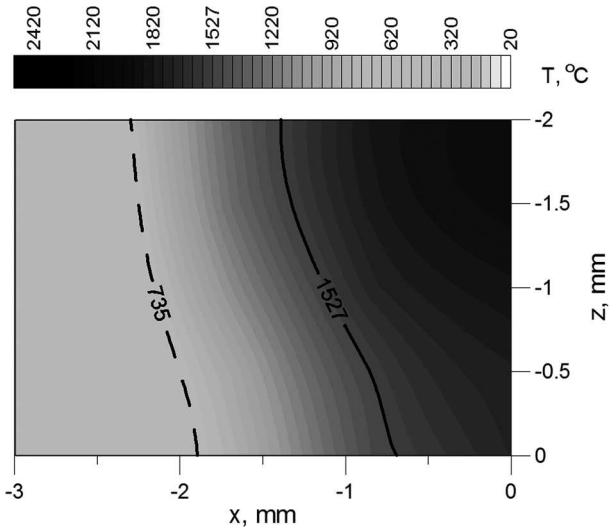

Fig. 5. Obtained temperature field in cross section of the joint

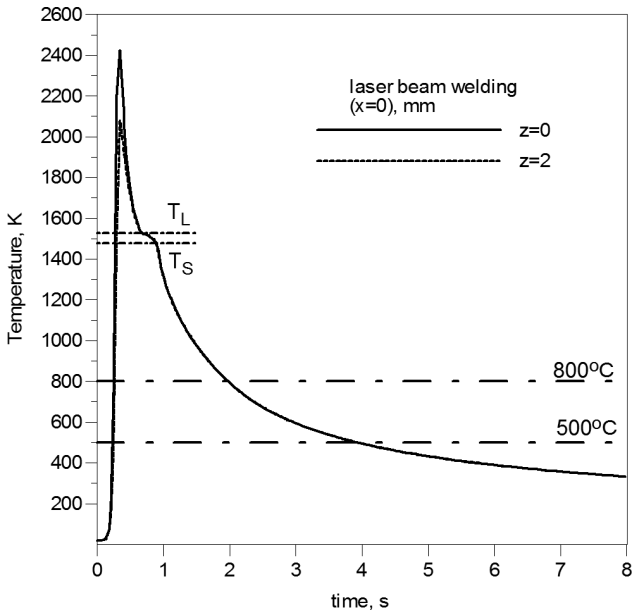

Fig. 6. Thermal cycles in chosen points of welded joint, at the top (z =0) and bottom (z =2mm) surface of the joint

Fig. 6 presents chosen thermal cycles in welding line at the top (z =0) and bottom (z =2 mm) surfaces of the joint. Solidus and liquidus temperatures are marked as well as the temperature range [800÷500]°C where cooling times (t_{8-5}) are estimated for analysis of phase transformations in solid state. It can be noticed that heat generated during melting and solidification of steel affects temperature distribution in the mushy zone and maximum temperatures are obtained in the centre of heat source activity zone.

For every thermal cycle in the weld and HAZ kinetics of phase transformations in solid state and isotropic strain is analyzed, depending on obtained heating and cooling rates. Figures 7 and 8 show kinetics of phase transformations in welding line (x=0) at the top (z =0) and bottom (z =2 mm) surfaces of the joint respectively with corresponding isotropic strain.

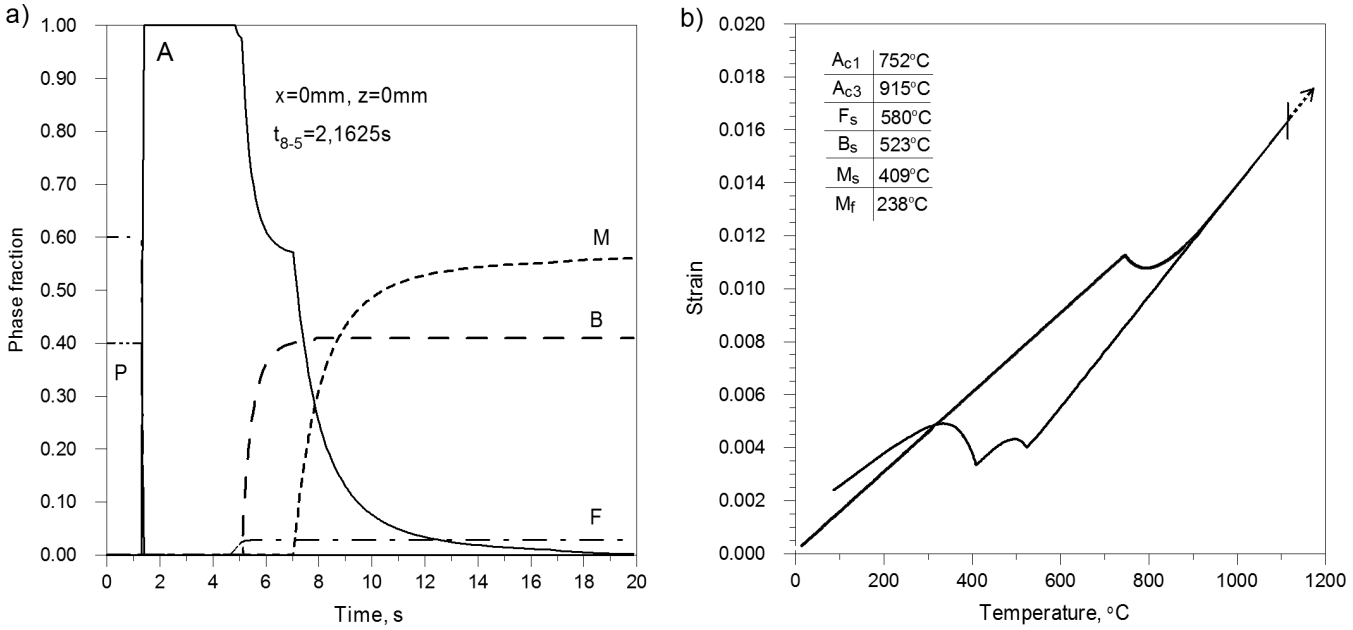

Fig. 7. Estimated a) kinetics of phase transformations for a point at the top surface of the joint (x =0, z =0) and corresponding b) thermal and structural strain

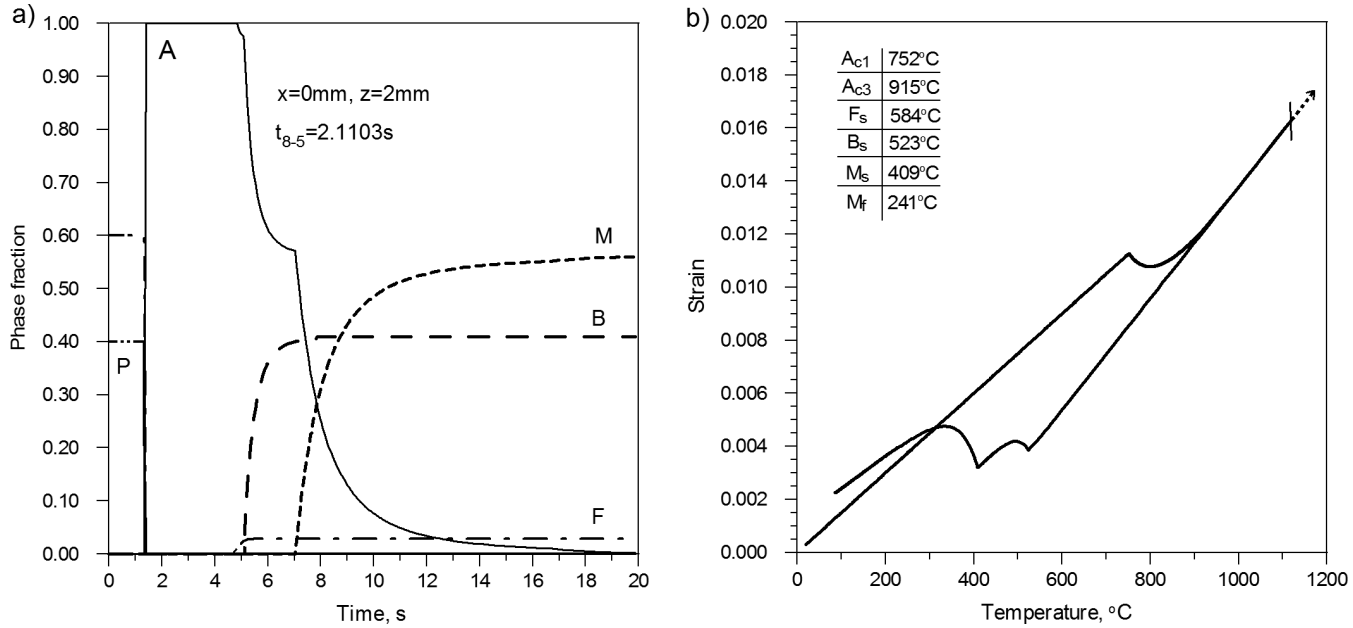

Fig. 8. Estimated a) kinetics of phase transformations for a point at the bottom surface of the joint (x =0, z =2 mm) and corresponding b) thermal and structural strain

In is observed that after solidification, laser welded joint is rapidly cooled to the ambient temperature, which results in partial hardening of the weld and heat affected zone. Cooling rates are decreasing in the material penetration direction, resulting in slight increase of martensite fraction.

5. Conclusions

Presented models for determination of movable heat source power distribution, kinetics of phase transformation, CHT and CCT diagrams as well as isotropic strain, implemented in additional subroutines used in Abaqus finite element analysis allowed numerical simulation of laser butt welding process.

Obtained temperature field in the cross-section of the weld (Fig. 5) allows the determination of fusion zone and heat affected zone geometry. Laser butt welded joint made of S355 steel is partially hardened in the weld and HAZ (Fig. 7-8), with martensite fraction up to 56% in welding line.

Developed in Abaqus FEA three-dimensional numerical model of laser butt welding allows the prediction of joint structural composition and isotropic deformation. Estimated properties are helpful in determining a proper set of process parameters necessary to obtain desired geometry of the weld and HAZ with a good quality of the joint.

REFERENCES

[1] C. Davies, Laser Welding: A practical guide; Abington Publishing; **261** (1992).
[2] J. Pilarczyk, M. Banasik, J. Stano, Technological applications of laser beam welding and cutting at the Instytut Spawalnictwa, Przeglad Spawalnictwa **5-6**, 6-10 (2006).
[3] M. Węglowski, S. Stano et al., Characteristics of Laser Welded Joints of HDT580X Steel Materials Science Forum **638-642**, 3739-3744 (2010).
[4] M.J. Torkamany, J. Sabbaghzadeh, M.J. Hamedi, Effect of laser welding mode on the microstructure and mechanical performance of dissimilar laser spot welds between low carbon and austenitic stainless steels, Mater Design **34**, 666-672 (2012).
[5] H. Long, D. Gery, A. Carlier, P.G. Maropoulos, Prediction of welding distortion in butt joint of thin plates, Mater Design **30**, 4126-4135 (2009).
[6] A. Bokota, W. Piekarska, Modeling of residual stresses in laser welding, Paton Weld. J **6**, 19-25 (2008).
[7] Z. Moumni, F. Roger, N. Thuy Trinh, Theoretical and numerical modeling of the thermomechanical and metallurgical behavior of steel, Int J Plasticity **27**; 414-439 (2011).
[8] V.I. Makhnenko, G.Y. Saprykina, Role of mathematical modelling in solving problems of welding dissimilar steels (Review), Paton Weld J **3**, 14-25 (2002).
[9] D. Gery, H. Long, P. Maropoulos, Effects of welding speed, energy input and heat source distribution on temperature variations in butt joint welding, J Mater Process Tech **167**, 393-401 (2005).

[10] W. P i e k a r s k a, M. K u b i a k, A. B o k o t a, Numerical simulation of thermal phenomena and phase transformations in laser-arc hybrid welded joints, Arch Metall Mater **56**, 409-421 (2011).

[11] A. A n c a, A. C a r d o n a, J. R i s s o et al., Finite element modeling of welding processes, Appl Math Model **35**, 688-707 (2011).

[12] S.A. T s i r k a s, P. P a p a n i k o s, Th. K e r m a n i d i s, Numerical simulation of the laser welding process in butt-joint specimens, J Mater Process Tech **134**, 59-69 (2003).

[13] SIMULIA Dassault System, Abaqus analysis user's manual, Version 6.7 (2007).

[14] SIMULIA Dassault System, Abaqus theory manual, Version 6.7 (2007).

[15] S.J. L e e, Y.K. L e e, Latent heat of martensitic transformation in a medium-carbon low-alloy steel, Scripta Mater **60**, 1016-1019 (2009).

[16] W. Z h a n g, B. W o o d, T. D e b R o y et al., Kinetic modeling of phase transformations occuring in the HAZ of C-Mn steel welds based on direct observations, Acta Mater **51**, 3333-3349 (2003).

[17] S. S e r a j z a d e h, Modelling of temperature history and phase transformations during cooling of steel, J Mater Process Tech **146**, 311-317 (2004).

[18] K.J. L e e, Characteristics of heat generation during transformation in carbon steels, Scripta Mater **40**, 735-742 (1999).

[19] W. P i e k a r s k a, Numerical analysis of thermomechanical phenomena during laser welding process. The temperature fields, phase transformation and stresses, Wydawnictwo Politechniki Częstochowskiej, Częstochowa (2007).

[20] A. B o k o t a, A. K u l a w i k, Model and numerical analysis of hardening process phenomena for medium-carbon steel, Arch Metall Mater **52**, 337-346 (2007).

[21] J. W i n c z e k, Modelling of heat affected zone in cylindrical steel elements surfaced by welding, Appl Math Model **36**, 1514-1528 (2012).

Received: 10 May 2012.